PHYSICAL REVIEW E VOLUME 58, NUMBER 3 SEPTEMBER 1998

Formation, motion, and decay of vectorial cavity solitons

U. Peschel, D. Michaelis, C. Etrich, and F. Lederer
Institut für Festkörpertheorie und Theoretische Optik, Friedrich-Schiller-Universität Jena, Max-Wien-Platz 1, 07743 Jena, Germany
(Received 20 January 1998; revised manuscript received 18 June 1998)

We show that symmetry breaking in vectorial intracavity second-harmonic generation is the prerequisite for the formation of cavity solitons. These solitons emerge as a result of self-organization of modulationally unstable polarization fronts. It is shown that truncated one-dimensional cavity solitons move because they lack the equilibrium of attracting and repelling forces. Collisions of various two-dimensional cavity solitons result in a rich diversity of final states. [S1063-651X(98)51409-2]

PACS number(s): 42.65.Tg, 03.40.Kf, 42.60.Da, 42.65.Ky

Stable localized states in nonlinear optical systems with spatial degrees of freedom attract growing interest. These spatial solitary waves or solitons represent a balance between linear dispersing effects, caused by spatial correlations as diffraction in continuous or coupling in discrete systems, and the action of some nonlinearity. Parametric solitons represent bound states of two or three field components locked by a quadratic interaction [1,2]. It was shown that they exist not only in Hamiltonian systems but also in dissipative ones as e.g. in externally driven cavities with intrinsic and radiation losses. Thus they can be termed cavity solitons. Cavity solitons were found to exist as one- and two-dimensional objects in optical parametric oscillators (OPOs) (down-conversion) [3,4] and in intracavity second harmonic (SH) generation (up-conversion) [5]. The situation where two fundamental harmonic (FH) components of orthogonal polarization generate a SH wave (vectorial interaction) is of particular interest [6,7]. Various types of cavity solitons were already found for other nonlinearities, e.g., for saturable focusing [8] and saturable absorbtive media [9], for semiconductors [10,11], and in the limit of nascent optical bistability in the vicinity of critical points [12]. Concerning intracavity vectorial second harmonic generation, it has been shown that for a symmetric input beyond a certain threshold intensity a spontaneous symmetry-breaking bifurcation takes place [13]. In this Rapid Communication, we show that this symmetry breaking can result in the formation of modulationally unstable topological solitons. However, we will demonstrate that these developing modulational instabilities (MIs) can, at least partially, be suppressed, and stationary as well as nonstationary localized structures can form. We show that localized structures in a dissipative optical environment can move and exhibit an amazing diverse collision behavior. We point out that the procedure we pursue can be applied for other nonlinear systems, e.g., with cross-phase modulation due to third-order nonlinearities that exhibit symmetry breaking as well [14,15] regardless of whether or not they are optical ones.

Here we assume that two orthogonally polarized FH waves with equal mean frequencies generate a SH wave of either polarization (type-II phase matching) in a high-finesse planar cavity (Fabry-Pérot resonator) with a quadratic nonlinear material. The model holds likewise for the case where the interaction of two input waves with different frequencies leads to the formation of a wave with the corresponding sum frequency. In contrast to the conventional scheme of an OPO, where the relevant effect is spontaneous down-conversion, we assume driving fields $E_{1/2}$ at the FH frequency. Our primary concern is the evolution of the emerging FH cavity fields $A_{1/2}$, whereas the SH cavity field B serves essentially as an idler required for quadratic interaction. In the good cavity limit the scaled evolution equations read as [16]

$$\left[i\frac{\partial}{\partial T} + \frac{\partial^2}{\partial X^2} + \frac{\partial^2}{\partial Y^2} + \Delta_A + i \right] A_j + A_{3-j}^* B = E_j, \quad j = 1,2,$$
$$\left[i\frac{\partial}{\partial T} + \frac{1}{2}\left(\frac{\partial^2}{\partial X^2} + \frac{\partial^2}{\partial Y^2} \right) + \Delta_B + i\gamma \right] B + A_1 A_2 = 0, \tag{1}$$

where T denotes the time scaled with respect to the FH photon lifetime in the cavity. The transverse coordinates are normalized with respect to the inverse angular linewidth of the FH resonance. Crucial parameters that control the optical response of the resonator are the respective detunings $\Delta_{A/B}$ from the resonances scaled with the FH resonance width and the ratio between the photon lifetimes γ. All intensities are normalized such that the coefficients in front of the nonlinear terms, viz., the effective quadratic susceptibility accounting for the field overlap and also for the mismatch of the wave numbers, become unity.

The normalized quantities can easily be related to the real world. This relation depends crucially on the finesse of the cavity, e.g., response time and spatial scales increase with the finesse, whereas the intensity scales decrease. A typical configuration could consist of a 500-μm-thick KTP crystal sandwiched between two mirrors with 95% reflectivity for both the FH and the SH waves. If the d_{31} coefficient is employed and phase matching occurs at a certain tilt at 1.06 μm, one obtains the length and time scales as 30 μm and 110 ps, respectively. Close to phase matching, $\gamma = 1$ holds. The driving intensity $|E_1|^2 = 1$ corresponds to 50 kW/cm^2.

Solving Eq. (1) we used different numerical codes. Stationary solutions of Eq. (1) were sought in taking advantage of a Newton iteration scheme based on a band matrix solver. For the full dynamical simulation we employed two different codes, viz., a 1+2-dimensional finite difference time domain procedure as well as a split-step fast-Fourier routine. The numerical grid consisted usually of 256×256 points. Because we were interested in localized structures on a

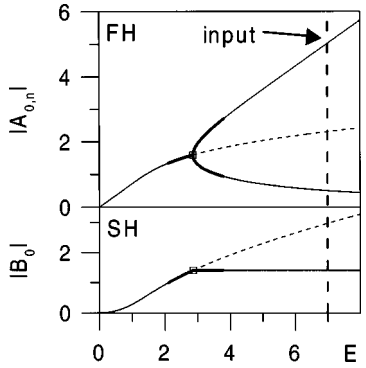

FIG. 1. Symmetry-breaking and modulational instabilities of the stationary plane wave solutions. Shown are the transmitted amplitudes vs the incident field E for a symmetric input and $\Delta_A=1, \Delta_B=1.5, \gamma=1$; thin solid (dashed) lines: stable (unstable) plane wave solutions; thick solid lines: modulationally unstable domains; squares; symmetry-breaking bifurcations.

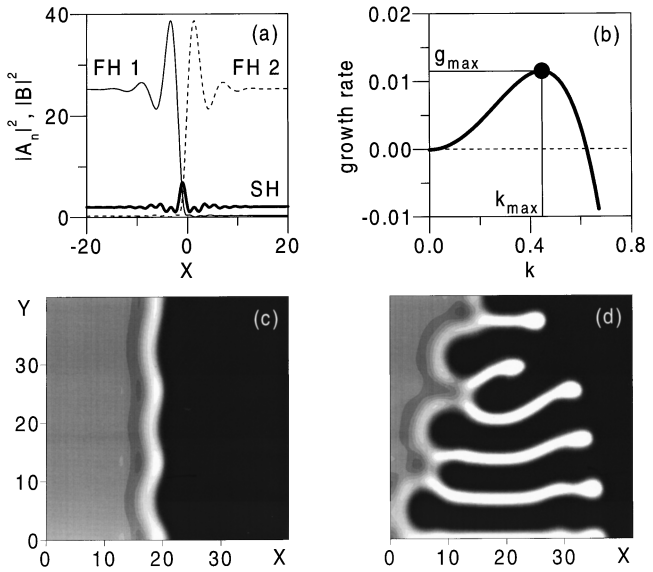

FIG. 2. One-dimensional solitons (polarization fronts) and their modulational instability in two dimensions; parameters as in Fig. 1 and $E=7$. (a) Topological solitons (polarization front) in the FH and bright soliton in the SH. (b) MI gain of the one-dimensional soliton. (c) Evolving snakelike instability of the polarization front ($T=320$) (d) Decay of the polarization front and emission of moving structures ($T=560$).

plane-wave background, the boundary conditions did not play a crucial role provided that the computing window was chosen large enough to avoid any interaction with the boundaries. In fact, both reflecting (derivative equal to zero) and periodic boundary conditions provided the same results.

As usual, the instabilities of stationary plane wave solutions $A_{10/20}$ and B_0 serve as a point of departure for the identification of transverse localized structures. Because we are particularly concerned with symmetry-breaking effects, we assume a symmetric input $E_1=E_2=E$ and express the stationary plane-wave solutions by their respective sum $S_0=(A_{10}+A_{20})/2$ and difference $D_0=i(A_{10}-A_{20})/2$. Then, in the stationary plane-wave limit Eqs. (1) simplify to

$$[\Delta_A+i]S_0+S_0^*B_0=E,$$

$$[\Delta_B+i\gamma]B_0+S_0^2+D_0^2=0, \tag{2}$$

$$[\Delta_A+i]D_0+D_0^*B_0=0.$$

Obviously, Eqs. (2) imply that in terms of sum and difference amplitudes, vectorial intracavity second-harmonic generation resembles the scalar case. One field (here S_0) generates the second harmonic, whereas the other field (here D_0) is exclusively excited via spontaneous down-conversion. Thus our scheme corresponds to an OPO but with a driving SH field generated via up-conversion of an additional FH field. For small input fields E, the SH is weak. Consequently no difference field is generated ($D_0=0$) and the case of scalar SH generation is recovered. Conversely, symmetry breaking ($D_0\neq 0$) occurs if the SH field B_0 matches the OPO threshold $|B_0|^2=\Delta_A^2+1$ [see the third of Eqs. (2)]. It is worth noting that for a further increase of the input amplitude the SH intensity remains locked to the threshold value (for more details see [8]). The respective bifurcation diagram is displayed in Fig. 1. In any case, the asymmetric state is single valued, although conventional continuous-wave bistability (S-shaped hysteresis loop) may occur on the symmetric branch before the symmetry-breaking bifurcation. Beyond the pitchfork bifurcation, the symmetric state is unstable against homogeneous perturbations. Although the asymmetric branches may again destabilize via modulational instabilities (thick solid lines in Fig. 1), a Hopf bifurcation, or running waves, here we will exclusively consider parameter domains where the asymmetric plane-wave solution is stable (perpendicular line in Fig. 1). There are two distinct but mathematically identical situations, viz., $A_1>A_2$ and $A_1<A_2$. Because these states can coexist, similarly to domains of different magnetization in a ferromagnetic material, the transition between them leads to the formation of a one-dimensional topological soliton [see Fig. 2(a)]. Recalling that the two FH amplitudes apply to perpendicular polarizations, the result is a polarization front. With only one transverse degree of freedom, say, x, as e.g. in a film waveguide resonator, this soliton is stable and it rests because of its symmetry with respect to an interchange of the two FH components. Accounting for the second transverse dimension (y), the polarization front [field structure $f_i^0(x)$, $i=A_1,A_2,B$] turns out to be modulationally unstable with respect to perturbations of the form $\delta f_i(x,k)\cos(ky+\varphi_0)$, which grow exponentially in time with the growth rate (MI gain) $g(k)$ [see Fig. 2(b)]. For $k=0$ the gain is zero because the one-dimensional case is recovered where the structure is stable and translational invariance holds. In this case, the linear eigenmode $\delta f_i(x,k=0)$ is the resulting trivial mode the shape of which corresponds to the derivative $[\delta f_i(x,k=0)=\partial f_i^0(x)/\partial x]$ of the polarization front. We found the shape of the linear eigenmode $\delta f_i(x,k)$ to vary only slightly with growing spatial frequencies k. Thus its exponential growth results mainly in a periodic shift or a snakelike instability of the entire front [Fig. 2(c)] and an ultimate decay [Fig. 2(d)].

In two-dimensional geometries, only finite structures can be excited. An asymmetric, but homogeneous, polarization distribution can be altered by a short local increase of that input field component that exhibits the weak cavity field. Accordingly, the front between two domains of different po-

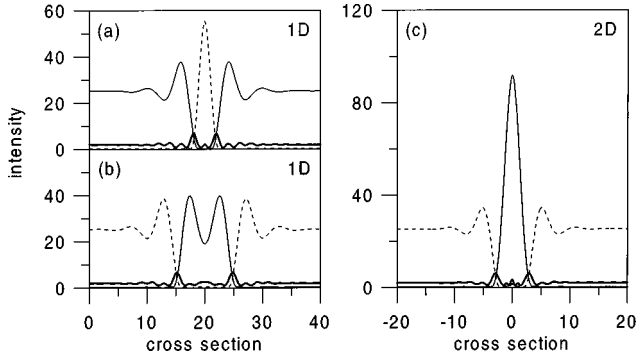

FIG. 3. Stable cavity solitons in a two-dimensional environment; parameters as in Fig. 2; (a) first-order one-dimensional soliton, (b) second-order one-dimensional soliton, (c) first-order two-dimensional soliton; dashed and thin solid lines; FH, bold line: SH.

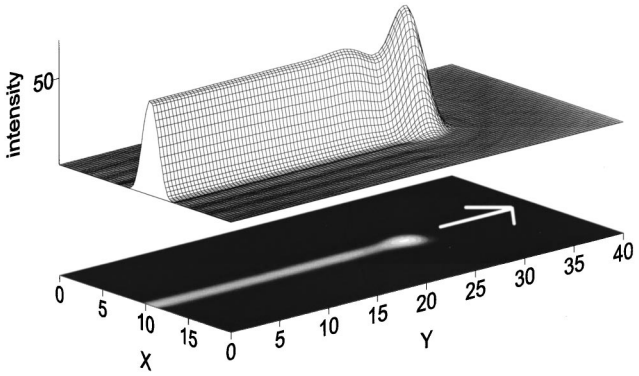

FIG. 4. Moving soliton (parameters as in Fig. 2).

larization is always bent somewhere. For a moderate bending (large radius) the modulational instability observed above manifests itself in a radial expansion of the bent structure. Comparing the curvature of a circular structure with that of a developing snakelike instability we derive the expansion velocity from the MI gain as

$$\nu_{\mathrm{exp}}(R) \cong g(k_{\mathrm{max}})/(k_{\mathrm{max}}^2 R), \tag{3}$$

where R is the radius of curvature and $g(k_{\mathrm{max}})$ the maximum growth rate arising at the spatial frequency k_{max}. Consequently, a circular domain of one polarization grows at the expense of the surrounding area with a velocity asymptotically approaching zero [see Eq. (3)]. As already mentioned, this scenario is typical for large radii where the field shape of the straight front is preserved and the bending can be compared with that induced by evolving modulational instabilities on a straight polarization front. For small radii or several interacting fronts, a stabilization can be achieved. To understand this, we look at the conservative counterparts of the cavity solitons we are dealing with. In many Hamiltonian systems, solitary waves with oscillating tails occur. It has been shown that, e.g., two such objects may form bound states due to an effective, oscillating potential caused by the mutual interference of their oscillating tails [17]. Although our system is non-Hamiltonian, we observe similar phenomena. Looking at the shape of the one-dimensional topological soliton in Fig. 2(a), we find all field components of a straight polarization front to exhibit exponentially decaying spatial oscillations. This periodic potential can capture another front. Constructive interference of two parallel fronts results in stable stripes or one-dimensional solitons of different orders according to the number of oscillations between the fronts [see Figs. 3(a) and 3(b)]. Two-dimensional stable localized structures can be formed if the polarization front is bent to form a circle with a small radius. Then the front interacts with its own oscillating tails [see Fig. 3(c)]. The stable and resting solitons of different order that arise represent an equilibrium between centrifugal and centripetal forces owing to the curvature and the periodic potential, respectively. Although different oscillations contribute to the periodic potential and determine the structure of the resulting solitons, the lowest-order solitons are defined by the constructive interference of the large-amplitude oscillations of the strong FH wave component. They exhibit a period of about

$$\lambda_1 \approx 2\pi/\mathrm{Re}(\sqrt{\Delta_A + i}). \tag{4}$$

and are strongly damped [see Fig. 2(a)] but determine the width of the peak of the lowest-order soliton.

Although one-dimensional solitons, shown in Figs. 3(a) and 3(b), are stable in two transverse dimensions, they require an infinite spatial domain to exist. This can be circumvented by bending the stripe to a large circle. But from a more realistic point of view, it is interesting to study how a truncated one-dimensional structure evolves. It can be easily excited by an elliptical beam. The final state is rapidly at-

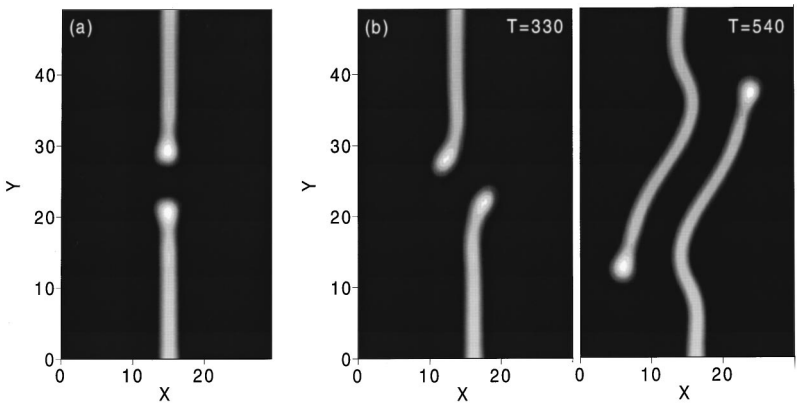

FIG. 5. Collision of moving cavity solitons (parameters as in Fig. 2). (a) central collision, (b) noncentral collision.

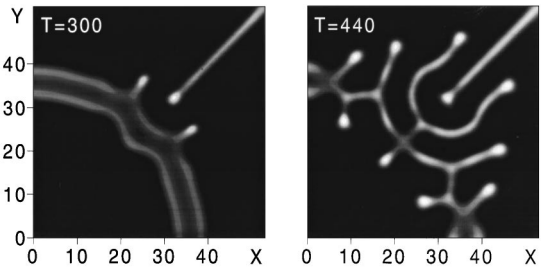

FIG. 6. Collision of a moving soliton with a one-dimensional resting second-order soliton (parameters as in Fig. 2).

tained and represents a stable soliton consisting of a growing stripe, identical to the one-dimensional soliton, and two-dimensional moving ''heads'' at both ends (see Fig. 4). In order to disclose the basic properties of such structures, we focus our attention on one side of the structure, keeping in mind that similar phenomena can be observed on the other side as well. Owing to the truncation of the stripe, there is no balance of forces at the head of the soliton. The force induced by the curvature remains uncompensated and the whole structure expands. The expansion velocity ν_{sol} is similar to that of a curved phase front of the same size and can be approximated for a first-order soliton by $\nu_{\mathrm{sol}} \approx \nu_{\mathrm{exp}}(\lambda_1/2)$. First-order moving solitons show a remarkable robustness. They are even emitted by decaying unstable structures such as polarization fronts [see Fig. 2(d)].

If solitons move, their interaction and collision behavior becomes a critical issue. We have performed various collision experiments and found the moving solitons to be very robust (see Fig. 5). A central collision of two moving solitons results in an unconventional final state, viz., prior to the actual collision, they halt and form a localized state consisting of two truncated resting solitons. After an off-axis collision they do not fuse or penetrate each other as observed in conservative systems; rather, they simply try to avoid close contact.

The situation changes drastically if less stable structures, i.e., higher-order resting solitons, are involved in the collision process. Here the impact of a moving soliton disturbs the intrinsic equilibrium that pins the structure together. As a consequence, new solitons are emitted where this can lead to the ultimate destruction of the colliding elements. Even if a one-dimensional second-order soliton is stabilized in two dimensions by bending it to a circle, its robustness is weak. Interaction with a moving truncated soliton induces complete decay starting at the collision site. Moving solitons are emitted, alternating between both sites. A treelike structure develops and starts to cover the whole plane with a roll pattern (see Fig. 6).

In conclusion, we have found that symmetry breaking occurs in vectorial intracavity second-harmonic generation. By combining the two different asymmetric states, a variety of localized structures can be formed. Resting and moving solitons of different orders are found. Truncated moving solitons can be understood as a symbiotic state consisting of one- and two-dimensional solitons. These moving solitons may be scattered at each other and at stationary localized structures. The scattering at higher-order solitons results in the emission of new solitons and in a partial or total destruction of the initial components.

[1] W. E. Torruellas, Z. Wang, D. J. Hagan, E. W. VanStryland, G. I. Stegeman, L. Torner, and C. R. Menyuk, Phys. Rev. Lett. **74**, 5036 (1995).

[2] R. Schiek, Y. Baek, and G. I. Stegeman, Phys. Rev. E **53**, 1138 (1996).

[3] S. Trillo, M. Haelterman, and A. Sheppard, Opt. Lett. **22**, 970 (1997).

[4] K. Staliunas and V. J. Sanchez-Morcillo, Opt. Commun. **139**, 306 (1997).

[5] C. Etrich, U. Peschel, and F. Lederer, Phys. Rev. Lett. **79**, 2454 (1997).

[6] C. Etrich, D. Michaelis, U. Peschel, and F. Lederer, Chaos Solitons Fractals (to be published).

[7] S. Longhi, Opt. Lett. **23**, 346 (1998).

[8] N. N. Rosanov and G. V. Khodova, J. Opt. Soc. Am. B **7**, 1057 (1990).

[9] W. J. Firth and A. J. Scroggie, Phys. Rev. Lett. **76**, 1623 (1996).

[10] M. Brambilla, L. A. Lugiato, F. Prati, L. Spinelli, and W. J. Firth, Phys. Rev. Lett. **79**, 2042 (1997).

[11] D. Michaelis, U. Peschel, and F. Lederer, Phys. Rev. A **56**, R3366 (1997).

[12] M. Tlidi, P. Mandel, and R. Lefever, Phys. Rev. Lett. **73**, 640 (1994).

[13] U. Peschel, C. Etrich, and F. Lederer, Opt. Lett. **23**, 500 (1998).

[14] J. B. Geddes, J. V. Moloney, E. M. Wright, W. J. Firth, Opt. Commun. **111**, 623 (1994).

[15] M. Haelterman, S. Trillo, and S. Wabnitz, J. Opt. Soc. Am. B **11**, 446 (1994).

[16] G.-L. Oppo, M. Brambilla, and L. A. Lugiato, Phys. Rev. A **49**, 2028 (1994).

[17] B. A. Malomed, Phys. Rev. E **47**, 2874 (1993).